PHYSICAL REVIEW D VOLUME 44, NUMBER 5 1 SEPTEMBER 1991

Color screening in hadron-hadron and hadron-nucleus collisions at high energies

V. V. Anisovich*
Bartol Research Institute, University of Delaware, Newark, Delaware 19716

L. G. Dakhno and V. A. Nikonov
Leningrad Nuclear Physics Institute, 188350 Gatchina, Leningrad District, U.S.S.R.
(Received 28 January 1991)

We consider color-screening effects in soft hadron-hadron and hadron-nucleus collisions at high energies using the idea of constituent (or dressed) quarks. It is shown that the quark color-screening hypothesis can be formulated as a sum rule for the elastic and inelastic quark-quark amplitudes. Taking into account color-screening effects, the cross sections $\sigma_{\rm tot}$ and $d\sigma_{\rm el}/dt$ are calculated for hadron-hadron and hadron-nucleus collisions.

I. INTRODUCTION

In Ref. [1] color-screening effects in soft hadronic processes at small and intermediate energies were discussed. The idea was first suggested in Ref. [2]. Here we extend these considerations into the region of higher energies $p \sim 100-500$ GeV/c where Pomeron exchange dominates in hadron-hadron scattering. Color-screening effects in hadron physics were originally discussed as a problem of hadron transparency at large p_T [3,4].

The problem of confinement is a problem of colored-particle interaction at comparatively large distances, i.e., a problem of soft hadronic physics. Two approaches to the soft hadronic processes can be specified: one of them explores the idea of bags with QCD quarks and gluons confined in the cavity. In another approach the hadron is treated as composite systems of massive constituent quarks and effective gluons.

The successes of hadron spectroscopy favor the idea of constituent quarks [5–7] with the mass of light constituent quarks u and d of the order of 300–400 MeV. A low-lying hadron in such an approach is a weakly bound system of constituent quarks. This suggests the impulse approximation for hadron collisions at high energies which leads to the additive quark model. The multiparticle production processes at high energies can be understood in terms of constituent quark collisions followed by the soft hadronization of quarks and soft color neutralization [8].

However, despite its remarkable achievements in describing global features of strong interactions, the additive quark model can only be regarded as a crude approximation, as it fails to describe some features of hadronic collisions. We think one of the reasons is the fact that the naive quark model does not take into account the effects of color screening.

In the present paper, starting with the constituent quarks, we consider color-screening effects in high-energy collision processes. Our considerations are very much reminiscent of dual topological unitarization (DTU) (see [8–10] and references therein). The novel feature is an emphasis on the t-channel structure of the Pomeron. Namely, the relative contribution of the impulse approximation and double scattering, or shadowing, diagrams depend strongly upon this structure. If the characteristic values of t in the Pomeron ladder are $t \sim 1-2$ (GeV/c)^2 (this is just the region of the most probable candidates for glueballs) then the leading contribution to the scattering amplitude comes from the impulse approximation. It is related to the small size of the Pomeron (see [8,11]). In this case color-screening diagrams are not negligible. Color screening becomes essential for small-size configurations of hadrons. This leads to a specific sum rule for the quark amplitudes, which is obtained in Sec. II.

Calculations of the elastic and total cross sections for hadron-hadron collisions, with color-screening effects taken into account, are carried out in Sec. III. These calculations show that color-screening corrections lead quite naturally to the ratio

$$\sigma_{\rm tot}(pp)/\sigma_{\rm tot}(\pi p) > \tfrac{3}{2} \tag{1}$$

while naive quark model calculations gave for this ratio a value less than $\frac{3}{2}$; this was a weak point of the additive quark model (see discussion in Ref. [8]).

High-energy hadron-nucleus collisions are discussed in Sec. IV. In the soft region of these processes color-screening calculations reveal a noticeable contribution of antishadowing corrections at high energies. Antishadowing corrections are necessary for the description of hadron-nucleus scattering in the framework of multiple-scattering theory, see Refs. [12,13].

At superhigh energies the total cross sections rise with energy. The growth in pp and $p\bar{p}$ cross sections at superhigh energies seems to be associated with the increase of QCD jets [14,15] (the modern treatment of this effect can be found in [16–22] and references therein). In Appendixes A and C we formulate some technical aspects which can help to consider screening at superhigh energies.

II. POMERON EXCHANGE AND COLOR SCREENING

We consider the region of not very high energies, $p \sim 100-500$ GeV/c, where hadron collisions are de-

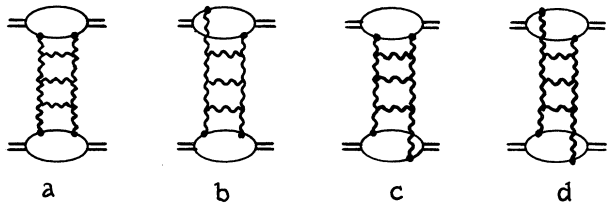

FIG. 1. Meson-meson scattering: gluonic ladder diagrams for the perturbative QCD Pomeron.

scribed by the Pomeron exchange.

As an example let us discuss the Pomeron in perturbative QCD [23,24]. The perturbative Pomeron is defined as a set of gluon ladder diagrams of the type shown in Fig. 1. QCD calculations are applicable in the region of large momentum transfer squared, t. At large t all the diagrams of Fig. 1 are of the same order according to the rule of $1/N_c$ expansion [25,26]. It is easy to show that they cancel each other when quark-antiquark distance tends to zero.

There are two types of Pomeron+meson coupling: (1) both gluons are coupled to the same quark, and (2) gluons are coupled with different quarks of the meson.

These two types of coupling are related to the two physical processes which are shown in Figs. 2(a) and 2(b).

The imaginary part of the diagram of Fig. 2(a) type is related to the total quark-quark cross section

$$\mathrm{Im}A_{qq}(0)\sim\sigma_{\mathrm{tot}}(qq) \tag{2}$$

while the imaginary part of diagrams of the Fig. 2(b) type gives the inclusive quark cross section

$$\mathrm{Im}A_{3q}(0)\sim\frac{d\sigma(qq\to qX)}{d^3k}\ . \tag{3}$$

These cross sections are connected by the relation

$$\sigma_{\mathrm{tot}}(qq)=\int d^3k\frac{d\sigma(qq\to qX)}{d^3k}\ . \tag{4}$$

This sum rule can be considered as a basis for the color-screening phenomenon. Because of Eq. (4) we will see below that the sum of diagrams of Figs. 1(a) and 1(b) vanishes when the relative quark-antiquark distance of the meson tends to zero.

As mentioned above, the use of the QCD Pomeron amplitude is justified in the region of large t only. The perturbative Pomeron expression violates analytic properties of the hadron scattering amplitude at small t. The latter has a nonzero imaginary part in the t channel at $|t|>4m_\pi^2$ (m_π is pion mass) while the nonzero imaginary part of perturbative QCD amplitude starts at $|t|>0$, just near the physical region. So, to use the QCD Pomeron in the soft scattering region, one needs some cutting procedure in the diagrams of Fig. 1 to eliminate the nonphysical imaginary part. Somehow it is equivalent to the introduction of effective gluon.

We will not discuss any special mechanism of the introduction of an effective gluon mass. We only use the fact that this phenomenon happens in some way.

For the description of the Pomeron in the region of small t we use general properties of the $1/N_c$ expansion. According to these rules the Pomeron is a cylinder-type gluonic net. Ladder diagrams of Fig. 1 give us the simplest example of such a net. The generalized form of these diagrams is shown in Fig. 3 where the Pomeron is presented as a gluonic cylinder with two types of coupling to meson quarks: either to both quarks or to one only. Here the situation is just the same as for ladder diagrams shown in Fig. 1. The diagrams of Figs. 3(a)–3(d) can be redrawn in terms of Reggeon exchanges—see Figs. 3(e)–3(h). The second type of Pomeron+quark coupling leads us to the three-Reggeon diagram [Figs. 3(f), 3(g)].

It seems to be reasonable that the main contribution to the diagrams of Figs. 3(f)–3(h) comes from the exchange of an effective gluon (G). Arguments in favor of this assumption are provided by the spectroscopy of low-lying hadrons: gluon-type interactions between quarks play the main role in binding constituent quarks. The problem of Reggeization of the gluon exchange was considered in Ref. [27].

Now let us turn to color screening in the meson-meson scattering amplitude in the region of nonperturbative QCD where the amplitude is defined by the diagrams of

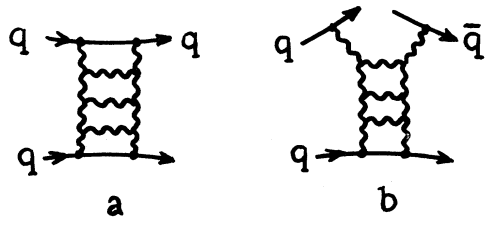

FIG. 2. Gluon ladder diagrams with two types of coupling of Pomeron with meson quarks.

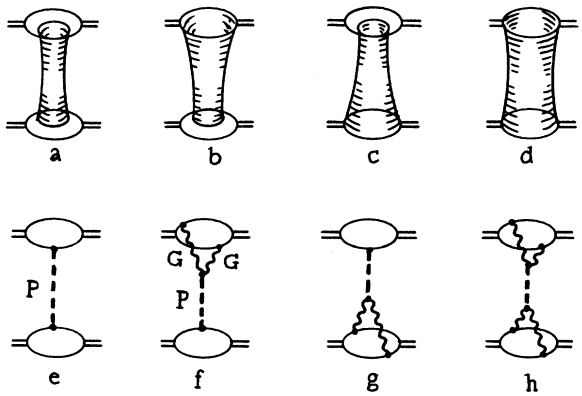

FIG. 3. Diagrams for meson-meson scattering amplitude with one-Pomeron exchange: (a)–(d) Pomeron is presented as a cylinder-type gluonic net, (e)–(h) the same diagrams are redrawn as Reggeon exchanges ($\mathcal{P}$ stands for Pomeron, G for Reggeized gluon).

Figs. 3(e)–3(h).

Consider the subprocesses shown in Figs. 4(a)–4(c), namely, quark-meson scattering. We require the situation in the soft region to be like in the region of perturbative QCD. Namely, the interaction of the Pomeron (or gluons of the Pomeron cylinder) with a meson vanishes when the distance between the constituent quark and antiquark of the meson tends to zero. This means that the sum of the diagrams [Figs. 4(a)–4(c)] tends to zero when $|\mathbf{r}_1-\mathbf{r}_2|\to 0$ (here $\mathbf{r}_1$ and $\mathbf{r}_2$ are coordinates of constituent quark and antiquark of the meson).

The diagrams of Figs. 4(a)–4(c) should be investigated in the context of the shadow correction analysis of the composite system. Detailed investigation of shadowing effects can be found, for example, in Refs. [8,28,29] and in the references therein. The amplitude corresponding to diagrams 4(a)–4(c) is

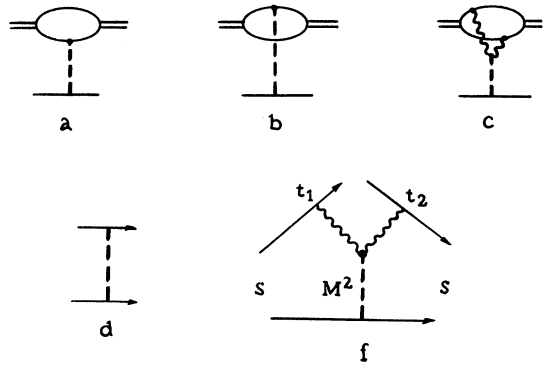

FIG. 4. (a)–(c) Diagrams for quark-meson scattering, (d) diagram describing elastic qq-scattering, (e) diagram for the transition $qq\bar{q}\to qq\bar{q}$ which determines inelastic shadowing in the diagram (c).

$$A(s,q^2)=[a_{qq}(q^2)+a_{q\bar{q}}(q^2)]F(q^2)-2\int_0^\infty dk_z\int d^2k_\perp F\left[4k_\perp^2+\frac{(M^2-m^2)^2}{p^2}\right]A_{3q}(s,q^2,t_1,t_2,M^2)\ . \tag{5}$$

Here $a_{qq}(q^2)$ and $a_{q\bar{q}}(q^2)$ are amplitudes for qq and $q\bar{q}$ scattering. For the Pomeron exchange $a_{qq}(q^2)=a_{q\bar{q}}(q^2)$. q^2 is the four-momentum transfer squared, $F(q^2)$ is meson form factor. The amplitude A_{3q} refers to the process of Fig. 4(e). Its amplitude depends on invariant variables which in the meson rest frame are

$$\begin{aligned} s&=2m_q p\ ,\\ t_1&=-(\mathbf{k}_\perp+\tfrac{1}{2}\mathbf{q})^2-k_z^2\ ,\\ t_2&=-(-\mathbf{k}_\perp+\tfrac{1}{2}\mathbf{q})^2-k_z^2\ ,\\ M^2&=2pk_z+m_q^2\ . \end{aligned} \tag{6}$$

p is the momentum of the incoming quark (the lower one in Figs. 4(a)–4(c), m_q is constituent quark mass, $\mathbf{k}=1/2(\mathbf{k}_1-\mathbf{k}_2)$. At small momentum transfer $q_z=0$, which was taken into account in Eq. (6).

The unitarity condition at $q^2=0$ gives

$$\begin{aligned} &\mathrm{Im}\,A(s,0)=\sigma_{\mathrm{tot}}(q+\mathrm{meson})\ ,\\ &\mathrm{Im}\,a_{qq}(s,0)=\sigma_{\mathrm{tot}}(qq)=\sigma_{\mathrm{tot}}(q\bar{q})\ ,\\ &\mathrm{Im}\,A_{3q}(s,0,-k^2,-k^2,M^2)=\frac{d\sigma(qq\to qX)}{d^2k_\perp dk_z}\ . \end{aligned} \tag{7}$$

At $q^2=0$ Eq. (5) turns into standard expression for the total cross section of composite system, inelastic screening taken into account [28,29]:

$$\sigma_{\mathrm{tot}}(q+\mathrm{meson})=2\sigma_{\mathrm{tot}}(qq)-2\int_{M^2_{\mathrm{thresh}}}^\infty dM^2\int d^2\kappa_\perp F\left[4\kappa_\perp^2+\frac{(M^2-m_q^2)^2}{p^2}\right]\frac{d\sigma(qq\to qX)}{d^2\kappa_\perp dM^2}\ . \tag{8}$$

In order to estimate the amplitude at $|\mathbf{r}_1-\mathbf{r}_2|\to 0$ one should rewrite Eq. (5) in the coordinate representation. For this purpose it is convenient to relate the meson form factor to the quark wave function:

$$F(q^2)=\int\frac{d^3k_1\,d^3k_2}{(2\pi)^3}\Psi(\mathbf{k}_1,\mathbf{k}_2)\Psi^*(\mathbf{k}_1+\mathbf{q},\mathbf{k}_2)\delta(\mathbf{k}_1+\mathbf{k}_2-\mathbf{P})=\int\frac{d^3k_{12}}{(2\pi)^3}\Psi(k_{12})\Psi^*(|\mathbf{k}_{12}+\tfrac{1}{2}\mathbf{q}|)\ . \tag{9}$$

$\mathbf{k}_1$ and $\mathbf{k}_2$ are the momenta of meson quark and meson antiquark. The meson wave function $\Psi(\mathbf{k}_1,\mathbf{k}_2)$ [or $\Psi(k_{12})$] depends on $\mathbf{k}_{12}=\frac{1}{2}(\mathbf{k}_1-\mathbf{k}_2)$ only. The corresponding wave function in r representation is

$$\Psi(\mathbf{k}_1,\mathbf{k}_2)=2^{3/2}\int d^3r_1\,d^3r_2\,e^{i\mathbf{k}_1\cdot\mathbf{r}_1+i\mathbf{k}_2\cdot\mathbf{r}_2}\Phi(\tfrac{1}{2}|\mathbf{r}_1-\mathbf{r}_2|)\delta^3(\mathbf{r}_1+\mathbf{r}_2)\ . \tag{10}$$

The normalization condition for $\Phi(\frac{1}{2}|\mathbf{r}_1-\mathbf{r}_2|)$ is

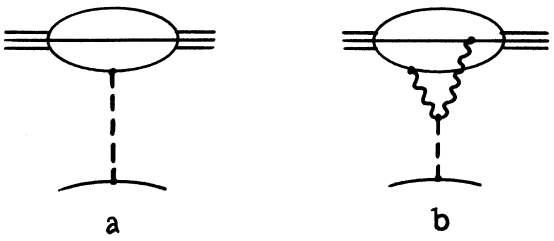

FIG. 5. Quark-baryon interaction due to Pomeron exchange.

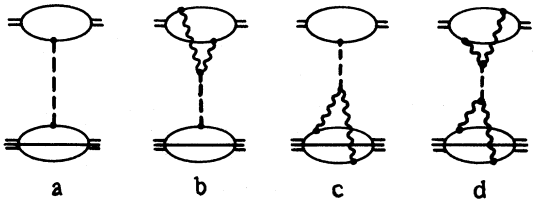

FIG. 6. Diagrams for meson-nucleon interaction.

$$\int d^3r_1\, d^3r_2\, \Phi^2(r_{12})\delta^3(\mathbf{r}_1+\mathbf{r}_2)=1\ . \tag{11}$$

Here we denote $\mathbf{r}_{12}=(\mathbf{r}_1-\mathbf{r}_2)/2$. The wave function $\Phi(r_{12})$ determines the meson form factor as

$$F(q^2)=\int d^3r_{12}\,\Phi^2(r_{12})e^{-i\mathbf{r}_{12}\mathbf{q}}\ . \tag{12}$$

The amplitude of Eq. (5) is rewritten as

$$A(s,q^2)=\int d^3r_{12}\,\Phi^2(r_{12})\left[2a_{qq}(q)e^{-i\mathbf{r}_{12}\mathbf{q}}-2\int_0^\infty dk_z\int d^2k_\perp e^{-i2\mathbf{k}\cdot\mathbf{r}_{12}}A_{3q}(s,q^2,t_1,t_2,M^2)\right]\ . \tag{13}$$

The hypothesis of color screening for meson quarks means that the expression in the large parentheses of Eq. (13) should be equal to zero at $r_{12}=0$. The following sum rule arises:

$$a_{qq}(q^2)=a_{q\bar{q}}(q^2)=\int_0^\infty dk_z\int d^2k_\perp\, A_{3q}(s,q^2,t_1,t_2,M^2)\ . \tag{14}$$

At $q^2=0$, when unitarity condition (7) is used, the sum rule turns into Eq. (4).

Consider now quark-baryon scattering through Pomeron exchange (see Fig. 5). The amplitude is defined by three impulse approximation terms [Fig. 5(a)] and three terms with triple-Reggeon interaction [Fig. 5(b)]:

$$A(s,q^2)=3a_{qq}(q^2)F_N(q^2)-3\int_0^\infty dk_z\int d^2k_\perp\, F_N^D(-\mathbf{k}+\tfrac{1}{2}\mathbf{q}_1,\mathbf{k}+\tfrac{1}{2}\mathbf{q}_2)A_{3q}(s,q^2,t_1,t_2,M^2)\ . \tag{15}$$

Here F_N^D is the nucleon difactor

$$F_N^D(q_1,q_2)=\int\frac{d^3k_1\,d^3k_2}{(2\pi)^3}\Psi^*(\mathbf{k}_1,\mathbf{k}_2,\mathbf{k}_3)\Psi(\mathbf{k}_1+\mathbf{q}_1,\mathbf{k}_2+\mathbf{q}_2,\mathbf{k}_3)\delta(\mathbf{k}_1+\mathbf{k}_2+\mathbf{k}_3-\mathbf{P})\ . \tag{16}$$

Let us stress that in Eq. (15) the amplitude A_{3q} is the same as for quark-meson scattering. But three-Reggeon interactions for mesons and baryons differ by the factor 2 because the gluon exchange is greater for the $q\bar{q}$ white state as compared to the color $\bar{3}$ state of qq. Just this factor is responsible for the fact that three baryon quarks do not interact with the Pomeron when all of them are at small distances ($r_{12}\to 0, r_{23}\to 0$). One can also see from Eq. (15) that two quarks, when they overlap, interact with the Pomeron as an antiquark.

Generalization of these sum rules for the super-high-energy region, where the amplitudes are of the Froissart-type, is discussed in Appendix A.

III. πp AND pp TOTAL AND DIFFERENTIAL CROSS SECTIONS

The pion-nucleon interaction amplitude is the sum of diagrams shown in Figs. 6(a)–6(d). The formulas related to each diagram are [notations I–IV correspond to Figs. 6(a)–6(d)]:

$$\begin{aligned}
&\mathrm{I}=6\sigma_{qq}F_\pi(q^2)F_N(q^2)e^{-(2G_{\mathcal{P}}+a'_{\mathcal{P}}\ln s)q^2}\ ,\\
&\mathrm{II}=-6F_N(q^2)e^{-(2G_{\mathcal{P}}+a'_{\mathcal{P}}\ln s)q^2}\int d^3\kappa\, F_\pi(4\kappa^2)A_{3q}(\kappa)\ ,\\
&\mathrm{III}=-6F_\pi(q^2)e^{-(2G_{\mathcal{P}}+a'_{\mathcal{P}}\ln s)q^2}\int d^3\kappa\, F_N^D(-\boldsymbol{\kappa}+\tfrac{1}{2}\mathbf{q},\boldsymbol{\kappa}+\tfrac{1}{2}\mathbf{q})A_{3q}(\kappa)\ ,\\
&\mathrm{IV}=\frac{6}{\sigma_{qq}}e^{-(2G_{\mathcal{P}}+a'_{\mathcal{P}}\ln s)q^2}\int d^3k\, F_\pi(4k^2)A_{3q}(k)\int d^3\kappa\, F_N^D(-\boldsymbol{\kappa}+\tfrac{1}{2}\mathbf{q},\boldsymbol{\kappa}+\tfrac{1}{2}\mathbf{q})A_{3q}(\kappa)\ .
\end{aligned} \tag{17}$$

Here F_π and F_N are pion and nucleon form factors and F_N^D is the nucleon difactor (corresponding expressions are given in Appendix B). The quark-quark scattering amplitude is parametrized as

$$a_{qq}=i\sigma_{qq}e^{-(2G_{\mathcal{P}}+a'_{\mathcal{P}}\ln s)q^2} . \tag{18}$$

$a'_{\mathcal{P}}$ is the Pomeron slope [$a'_{\mathcal{P}}\sim 0.25$ (GeV/c)$^{-2}$].

For the amplitude A_{3q} we have chosen the parametrization in the form

$$A_{3q}(\kappa^2)=V\left[\frac{M^2}{s}\right]^{\Delta}e^{-r^2\kappa^2} . \tag{19}$$

σ_{qq}, $G_{\mathcal{P}}$, V, Δ, and r^2 in Eqs. (17) and (19) are unknown parameters. M is invariant mass produced in the inelastic collision of quarks. Δ is a whole intercept of the three-Reggeon diagram [Fig. 4(e)], $\Delta=a-2\beta$, where a is the Pomeron intercept ($a=1$) and β is that of Reggeized gluon (according to the perturbative QCD estimations $\beta\cong 1$). The sum rule (14) provides an additional connection between parameters σ_{qq}, V, R^2 and Δ:

$$\sigma_{qq}-m_q V\frac{\pi}{r^2(1+\Delta)}=0 . \tag{20}$$

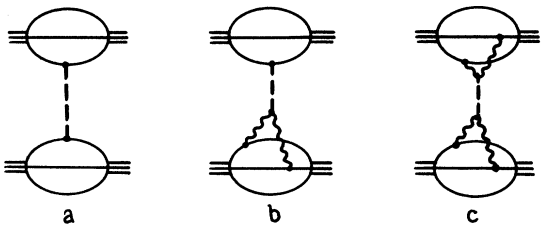

FIG. 7. Diagrams for proton-proton interaction.

The proton-proton scattering amplitude can be written similarly, corresponding diagrams are shown in Figs. 7(a)–7(c) (they are denoted as I, II, III):

$$\begin{aligned}
&\mathrm{I}=6\sigma_{qq}[F_N(q^2)]^2e^{-(2G_{\mathcal{P}}+a'_{\mathcal{P}}\ln s)q^2} ,\\
&\mathrm{II}=-18F_N(q^2)e^{-(2G_{\mathcal{P}}+a'_{\mathcal{P}}\ln s)q^2}\int d^3\kappa\, F_N^D(-\boldsymbol{\kappa}+1/2\mathbf{q},\boldsymbol{\kappa}+1/2\mathbf{q})A_{3q}(\kappa) ,\\
&\mathrm{III}=-\frac{9}{\sigma_{qq}}e^{-(2G_{\mathcal{P}}+a'\ln s)q^2}\left[\int d^3\kappa\, F_N^D(-\boldsymbol{\kappa}+1/2\mathbf{q},\boldsymbol{\kappa}+1/2\mathbf{q})A_{3q}(\kappa)\right]^2 .
\end{aligned} \tag{21}$$

Numerical calculations were carried out for the momenta $p_\pi=200$ GeV/c and $p_p=310$ GeV/c where the measured total cross sections are [30]

$$\sigma_{\pi p}=24.06\pm 0.04 \text{ mb}, \quad \sigma_{pp}=39.59\pm 0.07 \text{ mb} . \tag{22}$$

Our calculations provided the values for total cross sections $\sigma_{\pi p}=24.44$ mb and $\sigma_{pp}=39.26$ mb, the parameters are

$$\sigma_{qq}=4.8 \text{ mb}, \quad \Delta=-0.9, \quad r^2=0.141(\text{GeV}/c)^{-2} . \tag{23}$$

The obtained cross-section ratio is $\sigma_{pp}/\sigma_{\pi p}=1.61$. In Fig. 8 differential cross sections are shown for πp and pp calculated with the parameter $G_{\mathcal{P}}=0.83(\text{GeV}/c)^{-2}$, experimental data are taken from Ref. [31].

In the energy region under consideration ($p\sim 100$–500 GeV/c) we can restrict ourselves to the impulse approximation diagrams. However, at super-high energies it is necessary to take care to s-channel unitarity because of the growth of cross sections with energy. For this purpose it is convenient to use the impact parameter representation. In Appendix C we rewrite the impulse approximation diagram in the b representation and perform unitarization of the scattering amplitude in the eikonal approach.

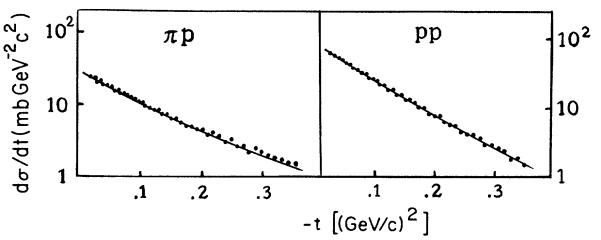

FIG. 8. Differential cross sections πp and pp: calculated values and experimental data [31].

IV. HADRON-NUCLEUS COLLISIONS

Here we describe the calculational technique for the hadron-nucleus amplitude with color-screening taken into account.

Let us consider meson-nucleus collisions. The scattering amplitude is defined as a set of diagrams like Fig. 9(a) with different number of rescatterings $n=1,\ldots,A$. The dashed block in Fig. 9(b) is the sum of diagrams [Figs. 9(c)–9(e)]. We denote it as $f(q_a,\kappa_a)$:

$$\begin{aligned}
f(q_a,\kappa_a)=&f_{qN}(q_a)(2\pi)^3\delta^3(\kappa_a-\tfrac{1}{2}q_a)\\
&+f_{\bar{q}N}(q_a)(2\pi)^3\delta^3(\kappa_a+\tfrac{1}{2}q_a)-2f_{qqN}(q_a,\kappa_a)
\end{aligned} \tag{24}$$

Here we use the scattering amplitudes which are adopted in the conventional multiple-scattering theory:

$$f_{qN}(q_a)=-ia_{qN}\ ,$$
$$f_{qqN}(\kappa,q_a)=-ia_{qqN}\ . \tag{25}$$

If we neglect the real part of the amplitude a_{qN} and a_{qqN} (which are small for Pomeron exchange) then

$$f_{qN}(0)=\sigma_{\rm tot}(qN)\ ,$$
$$f_{qqN}(\kappa,0)=(2\pi)^3\vartheta(\kappa_z)\frac{d\sigma}{d^3\kappa}(qN\to qX)\ . \tag{26}$$

The amplitude for meson-nucleus scattering is

$$f_{\pi A}(s,q^2)=\sum_{n=1}^{A}\frac{A!}{n!(A-n)!}f_n(s,q^2)\ . \tag{27}$$

Here f_n is the amplitude of diagram 9(a) and A is nuclear number. One can easily obtain f_n using standard formulas of the multiple-scattering theory (for example, see Chapters 3 and 4 of Ref. [8]). It is equal to

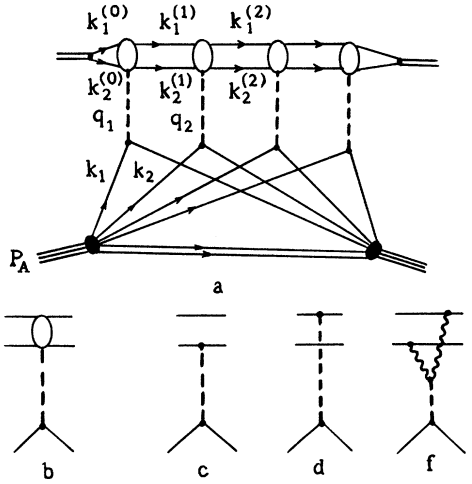

FIG. 9. (a) Diagram for the rescattering of pion quarks on nucleons of the nucleus. (b) Block for quark-nucleon interaction: processes c,d,e of Fig. 9.

$$f_n(s,q^2)=-2(-\tfrac{1}{2})^n\int\frac{d^3\kappa_1}{(2\pi)^3}\vartheta(\kappa_{1z})\cdots\frac{d^3\kappa_n}{(2\pi)^3}\vartheta(\kappa_{nz})\int\frac{d^3k_{12}}{(2\pi)^3}\Psi(k_{12})$$
$$\times\Psi\left[k_{12}+\sum_{a=1}^{n}\kappa_a\right]\int\prod_{j=1}^{A}\left[\frac{d^3k_j}{(2\pi)^3}\right](2\pi)^3\delta^3\left[\mathbf{P}_A-\sum_{j=1}^{A}\mathbf{k}_j\right]\Psi_A(\mathbf{k}_1\cdots\mathbf{k}_n,\mathbf{k}_{n+1}\cdots\mathbf{k}_A)$$
$$\times\Psi_A(\mathbf{k}_1+\mathbf{q}_1,\ldots,\mathbf{k}_n+\mathbf{q}_n,\mathbf{k}_{n+1},\ldots,\mathbf{k}_A)f(q_1,\kappa_1)\cdots f(q_n,\kappa_n)\ . \tag{28}$$

Ψ and Ψ_A are wave functions of the colliding meson and nucleus, $\mathbf{k}_1,\ldots,\mathbf{k}_A$ are the momenta of nucleons, and $\mathbf{k}_1^{(a)}$ and $\mathbf{k}_2^{(a)}$ are the momenta of quarks in intermediate states:

$$k_{12}=\tfrac{1}{2}(k_1^{(0)}-k_2^{(0)}),\quad k_1^{(1)}=k_1^{(0)}+\kappa_1-\tfrac{1}{2}q_1,\quad k_1^{(2)}=k_1^{(1)}+\kappa_2-\tfrac{1}{2}q_2,\ldots,$$
$$k_2^{(1)}=k_2^{(0)}-\kappa_1-\tfrac{1}{2}q_1,\quad k_1^{(2)}=k_1^{(1)}-\kappa_2-\tfrac{1}{2}q_2,\ldots\ . \tag{29}$$

In Eq. (28) let us introduce an additional integration

$$d^3\kappa\,\delta^3\left[\kappa-\sum_{a=1}^{n}\kappa_a\right] \tag{30}$$

and after that transform the amplitudes $f(\kappa_a,q_a)$ into the r representation

$$f(r_a,q_a)=\int\frac{d^3\kappa_a}{(2\pi)^3}e^{2i\mathbf{r}_a\cdot\kappa_a}f(\kappa_a,q_a)\ . \tag{31}$$

The amplitude $f_n(s,q^2)$ is rewritten as

$$f_n(s,q^2)=-2(-\tfrac{1}{2})^n\int d^3r\,f(r,q_1)\cdots f(r,q_n)F(r^2)F_A(q_1\cdots q_n)\frac{d^2q_1}{(2\pi)^2}\cdots\frac{d^2q_n}{(2\pi)^2}(2\pi)^2\delta^2\left[\mathbf{q}-\sum_{a=1}^{n}\mathbf{q}_a\right]\ . \tag{32}$$

Here $F_A(q_1\ldots q_n)$ is the nucleus n factor and $F(r^2)$ is meson form factor in the r representation:

$$F(r^2)=\int\frac{d^3\kappa}{(2\pi)^3}e^{-ir\cdot\kappa}F(\kappa^2)\ . \tag{33}$$

Remember that the meson difactor $D(q_1,q_2)$ can be expressed through the meson form factor $D(q_1,q_2)=F((\mathbf{q}_1-\mathbf{q}_2)^2)$.

The amplitude in Eq. (27) can be written in compact form if we use one-nucleon approximation for the nucleus wave function. In this case

$$F_A(q_q,\ldots,q_n)=F_N(q_1)\cdots F_N(q_n)\ ,$$
$$F_N(q)=\int\frac{d^3k}{(2\pi)^3}\Psi_N(\mathbf{k})\Psi_N^*(\mathbf{k}+\mathbf{q})\ , \tag{34}$$

where $\Psi_N(\mathbf{k})$ is one-nucleon wave function. The amplitude of pion-nucleus scattering $f_{\pi A}$ is equal to

$$f_{\pi A}(s,q^2)=2\int d^3r\,F(r^2)\times\int d^2b\,e^{i\mathbf{b}\cdot\mathbf{q}}\{1-[1-\tfrac{1}{2}\chi(\mathbf{b},\mathbf{r})]^A\}\ , \tag{35}$$

$$\chi(\mathbf{b},\mathbf{r})=\int\frac{d^2q_a}{(2\pi)^3}f(r,q_a)F_N(q_a)e^{-i\mathbf{b}\cdot\mathbf{q}_a}\ .$$

This is the final expression for meson-nucleus scattering amplitude where the color-screening effects of incident meson are taken into account. If we neglect color-screening effects [i.e., put $f_{qqN}=0$ in Eq. (24)], then Eq. (35) turns into the usual Glauber expression for the scattering of a two-particle composite system from a nucleus.

If A is large enough ($A>10$), we can simplify Eq. (35):

$$f_{\pi A}(s,q^2)\cong 2\int d^3r\,F(r^2)\times\int d^2b\,e^{i\mathbf{b}\cdot\mathbf{q}}(1-e^{-(A/2)\chi(\mathbf{b},\mathbf{r})})\ . \tag{36}$$

For small q (when $q\sim 1/R_A$) the q_a dependence in $f(r,q_a)$ can be neglected:

$$f(r,q_a)\cong f(r,0)=2\sigma_{\rm tot}(qN)-2\int d^3\kappa\,e^{2i\mathbf{r}\cdot\boldsymbol{\kappa}}\vartheta(\kappa_z)\times\frac{d\sigma}{d^3\kappa}(qN\to qX)\ . \tag{37}$$

In this case the function $\chi(\mathbf{b},\mathbf{r})$ is expressed through nucleon density $\rho(b^2)$:

$$A\chi(\mathbf{b},\mathbf{r})=f(r,0)\int db_z\,\rho(b^2)A=f(r,0)T(b)\ . \tag{38}$$

Here $T(b)$ is standard profile function with the normalization condition

$$\int d^2b\,T(b)=A\ . \tag{39}$$

In this case the amplitude $f_{\pi A}$ is equal to

$$f_{\pi A}(s,q^2)=2\int d^3r\,F(r^2)\times\int d^2b\,e^{i\mathbf{b}\cdot\mathbf{q}}(1-e^{-(1/2)f(r,0)T(b)}) \tag{40}$$

where $f(r,0)$ is defined by Eq. (37).

It is useful to compare Eq. (40) to the Glauber expression, where only meson-nucleon rescattering is taken into account:

$$f_{\pi A}^{\rm Glauber}(s,q^2)=2\int d^2b\,e^{i\mathbf{b}\cdot\mathbf{q}}\{1-\exp[-\tfrac{1}{2}\sigma_{\rm tot}(\text{meson}+N)T(b)]\} \tag{41}$$

According to the prescriptions of Secs. II and III, the total meson-nucleon cross section $\sigma_{\rm tot}(\text{meson}+N)$ should be written with a color screening term: namely,

$$\sigma_{\rm tot}(\text{meson}+N)=2\sigma_{\rm tot}(qN)-2\int\frac{d^3r}{(2\pi)^3}F(r^2)\int d^3\kappa\,e^{2i\mathbf{r}\cdot\boldsymbol{\kappa}}\vartheta(\kappa_z)\frac{d\sigma}{d^3\kappa}(qN\to qX)\ . \tag{42}$$

So the main difference between Eqs. (40) and (41) is the position of the operator $\int[d^3r/(2\pi)^3]F(r^2)$.

Using Eq. (40) we calculated πA total cross sections for Al, Cu, Pb with the values of $\sigma_{\rm tot}(qN)$ and $d\sigma/d^3\kappa(qN\to qX)$ obtained in the previous section. However it is not suitable to compare the results of our calculation directly to the experimental data. First, the data cover a broad energy range; hence, they are related to the different values of pion-nucleon cross sections. Second, they have systematic errors. The world data on pion-nucleus collisions were reanalyzed in Ref. [13] and systematic errors were eliminated, so we compare our results to those of Refs. [13,32].

Multiple-scattering theory operates with the language of hadrons and takes into account elastic, or Glauber, shadowing (fast moving particle is scattered on the nucleons of the target), inelastic shadowing [33,34] (diffractively produced resonances or a shower of secondaries are absorbed in the subsequent collision with the transition into initial particle) and inelastic antishadowing [35] (nondiffractive production of secondaries in the intermediate state). Hadron-nucleus scattering data were compared with multiple scattering theory in Refs. [12,13,28]. The results are as follows.

The Glauber screening in hadron-deuteron collision does not lead to correct values of the total πd cross sections. Agreement with the data is obtained after all screening effects were taken into account [28]: inelastic shadowing (diffractive and dissociation cross sections) and inelastic antishadowing (which is determined by certain triple-Reggeon diagram). The main contribution to screening is provided by the shadowing correction, while antishadowing is approximately three times smaller.

But there is another situation for hadron-^{4}He collisions: multiple-scattering theory does not agree with the experiments on total and differential $\pi\,^4$He and $p\,^4$He cross sections [12]. Analogous results were obtained for heavier nuclei: calculations [13] performed for $A=20$–200 gave

$$\frac{\sigma_{\rm tot}(\rm MST)}{\sigma_{\rm tot}(\rm expt)}-1\sim-(0.04\pm0.01)\ . \tag{43}$$

Calculations with Glauber correction differ from the data as well (the deviation has an opposite sign):

$$\frac{\sigma_{\rm tot}(\rm Gl)}{\sigma_{\rm tot}(\rm expt)}-1\sim(0.03\pm0.01)\ . \tag{44}$$

Our calculation for mesons scattered from heavy nuclei, which uses the language of constituent quarks and gluons with color screening taken into account, gives

$$\frac{\sigma_{\text{tot}}(\text{CS})}{\sigma_{\text{tot}}(\text{Gl})}-1=\begin{cases}-0.0073 & \text{for C}\ ,\\ -0.0082 & \text{for Al}\ ,\\ -0.0094 & \text{for Cu}\ ,\\ -0.0102 & \text{for Pb}\ .\end{cases} \tag{45}$$

It results in the ratio

$$\frac{\sigma_{\text{tot}}(\text{CS})}{\sigma_{\text{tot}}(\text{expt})}-1\sim 0.02\pm 0.01\ . \tag{46}$$

We see that calculations with color screening are not far from the experimental data.

V. CONCLUSION

We provide a description of hadron-hadron and hadron-nucleus collisions which backs up experimental data at high energies. Color screening of constituent quarks is taken into account, which leads naturally to the ratio $\sigma_{\text{tot}}(pp)/\sigma_{\text{tot}}(\pi p)\sim 1.6$. Let us stress that in naive quark model there were difficulties with this value: in the impulse approximation this ratio is $\frac{3}{2}$ and Glauber screening results in the diminishing of this value.

Our description of πN and NN scattering allowed us to fix the parameters of the quark-quark amplitudes and to use them for the calculation of hadron-nucleus collisions in the framework of multiple-scattering theory. Multiple-scattering theory, applied to the description of the high-energy hadron-nucleus collisions, may operate with two equivalent languages—hadron language and that of constituent quarks and gluons. As was mentioned above, calculations with the help of hadron language were not successful in describing hadron collisions with ^{4}He and heavy nuclei at high energies. At the same time, using the language of constituent quarks and gluons and taking into account color screening for the incident hadron, we obtain values of the total cross sections which are in the proximity of the experimental data.

We transform our results to the hadron language and conclude that in hadron-nucleus scattering the production and absorption of showers with effective masses $M^2\sim s(Rm_N)^{-1}$ are important processes (here m_N is nucleon mass, M is mass of shower, s is invariant energy squared of system of incident hadron plus nucleon and R is the average distance between nucleons in the nuclei). The production of showers with comparatively small masses leads to screening effects [33], while at larger masses antishadowing [35] becomes important. In hadron-deuteron scattering the region of large masses is cut by the deuteron form factor. As to the region of non-large masses (the region of diffractive dissociation) one can carry out calculations using the results of three-Reggeon analysis which are trustworthy enough for this use. Hence, inelastic screening in hadron-neutron scattering is calculated with sufficient accuracy. At the same time analogous calculations for ^{4}He and heavier nuclei faced a disagreement with the experimental data. The reasons could be the following: (i) the increase of antishadow effects connected with the contribution of large values of M^2, (ii) influence of the non-nucleonic degrees of freedom (according to the estimation of Refs. [12,13] to explain the discrepancy between the calculated and experimental data one needs an admixture of multiquark bag of the order of $\sim 10-15\,\%$).

If the hypothesis about duality of hadron and quark languages is assumed, then our calculations clarify the situation to certain extent. We see that in a sense color screening is equivalent to antishadowing effects. The proximity of our results to the data provides arguments that antishadowing, due to the large M^2 region, is underestimated in the calculations made with the hadron language. So the antishadowing should play a more important role in hadron-nucleus collisions. At the same time, our calculations deviate slightly $(1-3\,\%)$ from the experiment which leaves room for non-nucleonic degrees of freedom in nuclei which were not taken into account here.

Our considerations show that color-screening effects are essential in soft processes at high energies. Investigation of color-screening effects in other processes, especially in the hadron diffractive dissociation and low-x deep-inelastic scattering, seems to be important.

ACKNOWLEDGMENTS

The authors are grateful to R. S. Fletcher, T. K. Gaisser, P. Kroll, L. N. Lipatov, N. N. Nikolaev, H. Pirner, M. G. Ryskin, and T. S. Stanev for useful remarks and discussions. One of us (V.V.A.) thanks N. F. Ness for the hospitality at the Bartol Research Institute where this paper was finished.

APPENDIX A

It is rather simple to make a generalization of the sum rule (14) for the region of superhigh energies when the quark-quark interaction is carried out not with the exchange of Pomeron but with that of Froissaron. In the diagrams 4(a) and 4(b) one should replace Pomeron by Froissaron. Let us check out that this procedure leads us to the self-consistent equation. Equation (14) is written now as

$$i\ln^2 s A_{qq}(q^2)e^{-a'q^2\ln^2 s}-i\int_{M_{\text{th}}^2}^{s}\frac{dM^2}{s}\left[\frac{s}{M^2}\right]^{2\beta-1}\ln^2 M^2\int d^2k_\perp B_{3q}(t_1,t_2,q^2)\exp\left[-a'q^2\ln^2 M^2+\beta'(t_1+t_2)\ln\frac{s}{M^2}\right]=0\ , \tag{A1}$$

where β is Reggeized gluon intercept $\beta<1$. After the replacement $y=M^2/s$ the second term in the right-hand side of Eq. (A1) at $\ln s\gg 1$ and $q^2\ln^2 s\sim 1$ reads

$$-i\ln^2 s e^{-a'q^2\ln^2 s}\int_0^1 \frac{dy}{y^{2\beta-1}}\int d^2k_\perp B_{3q}(t_1,t_2,q^2)\exp\left[-\beta'(\tfrac{1}{2}q^2+2k_\perp^2)\ln\frac{1}{y}\right]. \tag{A2}$$

We see that s-dependent factors are the same for both terms, so we have the sum rule for the amplitudes $A_{qq}(q^2)$ and $B_{3q}(t_1,t_2,q^2)$:

$$A_{qq}(q^2)=\int_0^1 \frac{dy}{y^{2\beta-1}}\int d^2k_\perp B_{3q}(t_1,t_2,q^2)\exp\left[-\beta'(\tfrac{1}{2}q^2+2k_\perp^2)\ln\frac{1}{y}\right]. \tag{A3}$$

APPENDIX B

In our calculations we use the wave functions as a sum of two exponents

$$\Psi_\pi=a_\pi e^{-\gamma_\pi k^2}+b_\pi e^{-\delta_\pi k^2}, \tag{B1}$$

where $\mathbf{k}=\frac{1}{2}(\mathbf{k}_1-\mathbf{k}_2)$, and

$$\Psi_N=\sum_i a_i \exp\left[-\gamma_i\sum_{em}k_{em}^2\right] \tag{B2}$$

where $\mathbf{k}_{em}=\frac{1}{2}(\mathbf{k}_e-\mathbf{k}_m)$. The corresponding form factors are

$$F_\pi(q^2)=\frac{1}{8\pi^{3/2}}\left[\frac{a_\pi^2}{(2\gamma_\pi)^{3/2}}\exp\left[-\frac{\gamma\pi}{8}q^2\right]+\frac{2a_\pi b_\pi}{(\gamma_\pi+\delta_\pi)^{3/2}}\exp\left[-\frac{\gamma_\pi\delta_\pi}{4(\gamma_\pi+\delta_\pi)}q^2\right]+\frac{b_\pi^2}{(2\delta_\pi)^{3/2}}\exp\left[-\frac{\delta_\pi}{8}q^2\right]\right], \tag{B3}$$

$$F_N(q^2)=\frac{1}{24\sqrt{3}(2\pi)^3}\left[\frac{a_N^2}{8\gamma_N^3}\exp\left[-\frac{\gamma_N}{3}q^2\right]+\frac{2a_N b_N}{(\gamma_N+\delta_N)^3}\exp\left[-\frac{2}{3}\frac{\gamma_N\delta_N}{\gamma_N+\delta_N}q^2\right]+\frac{b_N^2}{8\delta_N^3}\exp\left[-\frac{\delta_N}{3}q^2\right]\right]. \tag{B4}$$

Proton difactor is

$$D_N(q_1,q_2)=\frac{1}{24\sqrt{3}(2\pi)^3}\left[\frac{a_N^2}{8\gamma_N^3}\exp\left[-\frac{\gamma_N}{3}(q_1^2+q_2^2-\mathbf{q}_1\mathbf{q}_2)\right]+\frac{2a_N b_N}{(\gamma_N+\delta_N)^3}\exp\left[-\frac{2}{3}\frac{\gamma_N\delta_N}{\gamma_N+\delta_N}(q_1^2+q_2^2-\mathbf{q}_1\mathbf{q}_2)\right]+\frac{b_N^2}{8\delta_N^3}\exp\left[-\frac{\delta_N}{3\delta_N^3}(q_1^2+q_2^2-\mathbf{q}_1\mathbf{q}_2)\right]\right]. \tag{B5}$$

Here

$$a_\pi=105.633,\quad \gamma_\pi=50.87,\quad b_\pi=5.886,\quad \delta_p=5.39, \tag{B6}$$

$$a_N=7307.8,\quad \gamma_N=11.36,\quad b_N=502.4,\quad \delta_N=2.24.$$

All values are in GeV^{-2}. These values correspond to the standard pion and proton radii squared $\langle r_\pi^2\rangle=10\ \mathrm{GeV}^{-2}$ and $\langle r_N^2\rangle=17\ \mathrm{GeV}^{-2}$ and the behavior of form factors $F_\pi^{(q^2)}\simeq(1-q^2/0.5)^{-1}$ and $F_N(q^2)\simeq(1-q^2/0.71)^{-2}$ at $q^2\lesssim 0.8\ \mathrm{GeV}^2$.

APPENDIX C

Here we rewrite the formulas for the scattering amplitude in the impact-parameter representation and show how to provide s-channel unitarization. We consider as an example meson-meson scattering $(1+2\to 1+2)$. The impulse approximation amplitude of Fig. 10(a) is

$$F_{12\to 12}(q^2)=4\sigma_{qq}f_1(q^2)f_2(q^2)e^{-(2G_{\mathcal{P}}+\alpha'\ln s)q^2}. \tag{C1}$$

Let us introduce the energies squared s_1 and s_2 which are related to s as $s_1 s_2=sm_0^2$, we put below $m_0=1$ GeV. Then the amplitude $F_{12\to 12}$ can be written as

$$F_{12\to 12}^{(\mathrm{IA})}(q^2)=4\sigma_{qq}f_1^{\mathcal{P}}(q^2)f_2^{\mathcal{P}}(q^2), \tag{C2}$$

$$f_e^{\mathcal{P}}(q^2)=F_e(q^2)e^{-(G_{\mathcal{P}}+\alpha'\ln s_e)q^2}. \tag{C3}$$

Let us transform $f_e^{\mathcal{P}}(q^2)$ in the impact-parameter representation taking into account that at high energies $\mathbf{q}\simeq\mathbf{q}_\perp$:

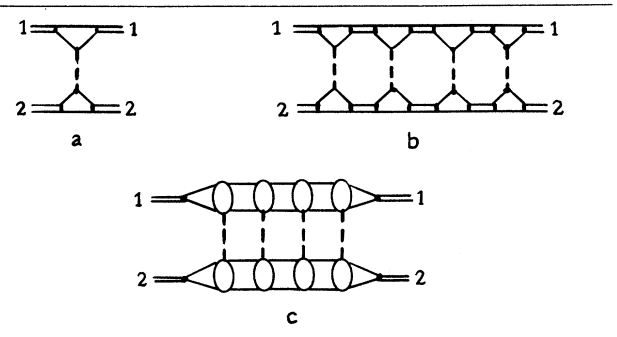

FIG. 10. Meson-meson scattering: (a) Impulse approximation diagram. (b) An example of a diagram sum of which leads to Eq. (C15) where only initial meson rescatterings are taken into account. (c) An example of a diagram where all intermediate states are taken into account. The sum of such type diagrams leads to Eq. (C20).

$$f_e^{\mathcal{P}}(q^2)=\int d^2b\, e^{iq\cdot b}\rho_e^{\mathcal{P}}(\mathbf{b})\ , \tag{C4}$$

$$\rho_e^{\mathcal{P}}(\mathbf{b})=\int d^2r_\perp F_e(\mathbf{r}_\perp)\rho_{\mathcal{P}}(\mathbf{b}-\mathbf{r}_\perp) \tag{C5}$$

where

$$F_e(\mathbf{r}_\perp)=\int \frac{d^2q}{(2\pi)^2}e^{i\mathbf{q}\cdot\mathbf{r}_\perp}F_e(q^2)\ , \tag{C6}$$

$$\rho_{\mathcal{P}}(\mathbf{b}')=\int \frac{d^2q}{(2\pi)^2}e^{i\mathbf{q}\cdot\mathbf{b}'}e^{-(G_{\mathcal{P}}+\alpha'\ln s_e)q^2}\ . \tag{C7}$$

$F_e(\mathbf{r})$ gives the density of the meson quarks at the fixed impact parameter $\mathbf{r}_\perp$ while $\rho_{\mathcal{P}}(\mathbf{b})$ is related with the density of partons in the Pomeron ladder. Then the amplitude of Eq. (C1) can be written as

$$F_{12\to 12}^{(\mathrm{IA})}(q^2)=\int d^2b\, e^{iq\cdot b}\ , \tag{C8}$$

$$A(\mathbf{b})=\int d^2b_1 d^2b_2\delta(\mathbf{b}-(\mathbf{b}_1-\mathbf{b}_2))\rho_1^{\mathcal{P}}(\mathbf{b}_1)\rho_2^{\mathcal{P}}(\mathbf{b}_2)\ .$$

In order to take into account color-screening effects we should make the replacement in Eq. (C3):

$$f_e^{\mathcal{P}}(q^2)\to f_e^{\mathrm{CS}}(q^2)=F_e(q^2)e^{-i(G_{\mathcal{P}}+\alpha'\ln s_e)q^2}-\frac{1}{\sigma_{qq}}\int d^3\kappa\, F_e(4\kappa^2)A_{3q}(\kappa,q)\ . \tag{C9}$$

In the framework of the parametrization for A_{3q} used in Sec. III we have

$$f_e^{\mathrm{CS}}(q^2)=\int d^2b\, e^{i\mathbf{b}\cdot\mathbf{q}}\rho_e^{\mathrm{CS}}(\mathbf{b})\ , \tag{C10}$$

$$\rho_e^{\mathrm{CS}}(\mathbf{b})=\int d^2r_\perp\rho(\mathbf{b}-\mathbf{r}_\perp)\left[F_e(\mathbf{r}_\perp)-(1+\Delta)\int_0^1 dy\, y^{\Delta+1}\int dr_z\,\Phi_e^2(r^2)e^{i2m_q y r_z}e^{-r_\perp^2/r_0^2}\right]\ . \tag{C11}$$

If the size of meson is not large and Δ is close to -1 then $\exp(i2m_q y r_z)\simeq 1$. In this case the expression in large parentheses of the right-hand side of Eq. (C11) can be simplified:

$$\rho_e^{\mathrm{CS}}(\mathbf{b})=\int d^2r_\perp F_e(\mathbf{r}_\perp)\left[\rho(\mathbf{b}-\mathbf{r}_\perp)-\rho(\mathbf{b})\exp\left[-\frac{r_\perp^2}{r_0^2}\right]\right]\ . \tag{C12}$$

The scattering amplitude with one-Pomeron exchange and color-screening effects taken into account is now equal to

$$F_{12\to 12}^{\mathrm{CS}}(q^2)=\int d^2b\, e^{i\mathbf{b}\cdot\mathbf{q}}4\sigma_{qq}A(\mathbf{b})\ , \tag{C13}$$

$$A(\mathbf{b})=\int d^2b_1\, d^2b_2\,\delta(\mathbf{b}-(\mathbf{b}_1-\mathbf{b}_2))\rho_1^{\mathrm{CS}}(\mathbf{b}_1)\rho_2^{\mathrm{CS}}(\mathbf{b}_2)\ . \tag{C14}$$

It is easy to perform the s-channel unitarization of the scattering amplitude taking into account all the rescattering of the Fig. 10(b) type with the use of the standard eikonal technique. The amplitude in this is equal to

$$F_{12\to 12}^{\mathrm{CS}}(q^2)=2\int d^2b\, e^{i\mathbf{b}\cdot\mathbf{q}}(1-e^{-\chi(\mathbf{b})/2})\ , \tag{C15}$$

$$\chi(\mathbf{b})=4\sigma_{qq}A(\mathbf{b})\ . \tag{C16}$$

In order to take into account all intermediate states in the diagrams of Fig. 10(b) type it is convenient to expand Eq. (C15) in the set of χ. We have terms such as

$$-\frac{(-\frac{1}{2})^k}{k!}\chi(\mathbf{b})\chi(\mathbf{b})\cdots\chi(\mathbf{b})\ . \tag{C17}$$

The summing over all intermediate states means the replacement

$$\chi(\mathbf{b})\chi(\mathbf{b})\ldots\chi(\mathbf{b})\to\sum_{\substack{m,m',\ldots\\ n,n',\ldots}}\chi_{2n}^{1m}(\mathbf{b})\chi_{nn'}^{mm'}(\mathbf{b})\ldots\chi_{n'''2}^{m'''1}(\mathbf{b}) \tag{C18}$$

where indices $m,m',\ldots$ and $n,n',\ldots$ refer to all quark-antiquark meson states. The functions $\chi_{nn'}^{mm'}$ are determined now by the above formulas with the replacement $F_1(r_\perp)\to F_{mm'}(r_\perp)$ and $f_2(r_\perp)\to F_{nn'}(r_\perp)$.

If we assume that for quark-antiquark wave functions the completeness condition can be written in the usual form

$$\sum_{m'}F_{mm'}(r_\perp)F_{m'm''}(r_\perp')=\delta^3(r_\perp-r_\perp')F_{mm''}(r_\perp)\ . \tag{C19}$$

In the terms such as (C18) the summing can be easily performed and we have instead of the Eqs. (C15) and (C16) the expressions

$$F_{12\to 12}^{\mathrm{CS}}(q^2)=2\int d^2b\, e^{i\mathbf{b}\cdot\mathbf{q}}\int dR_1 dR_2\Phi_1^2(\tfrac{1}{2}|\mathbf{r}_1-\mathbf{r}_1'|)\Phi_2^2(\tfrac{1}{2}|\mathbf{r}_2-\mathbf{r}_2'|)(1-e^{-(1/2)\chi(\mathbf{R}_1,\mathbf{R}_2,\mathbf{b})}) \tag{C20}$$

where

$$\begin{aligned}&dR_i=d^2r_i\, d^2r_i'\,\delta(\mathbf{r}_i+\mathbf{r}_i')\ ,\\ &\chi(\mathbf{R}_1,\mathbf{R}_2,\mathbf{b})=\sigma_{qq}\int d^2b_1\, d^2b_2\,\rho(\mathbf{r}_1,\mathbf{r}_1',\mathbf{b}_1)\rho(\mathbf{r}_2,\mathbf{r}_2',\mathbf{b}_2)\delta(\mathbf{b}-(\mathbf{b}_1-\mathbf{b}_2))\ ,\\ &\rho_1(\mathbf{r}_1,\mathbf{r}_1',\mathbf{b}')=\left[\rho(\mathbf{b}_1-\mathbf{r}_1)+\rho(\mathbf{b}_1-\mathbf{r}_1')-2\rho(\mathbf{b}_1)\exp\left[-\frac{(\mathbf{r}_1-\mathbf{r}_1')^2}{4r_0^2}\right]\right]\ .\end{aligned} \tag{C21}$$

Here r_i and r_i' are impact parameters of the quark and antiquark in meson i. The structure of the Eq. (C20) is quite similar to that of the Eq. (37) for meson-nucleus amplitude.

At superhigh energies $\chi(\mathbf{R}_1,\mathbf{R}_2,\mathbf{b})$ should be referred to as χ(soft). The value of $\chi_{\rm QCD}$ related to minijet production should be added in (C20) as an additional term $\chi(\text{soft})\rightarrow\chi(\text{soft})+\chi_{\rm QCD}$.

---

*Permanent address: Leningrad Nuclear Physics Institute, 188350 Gatchina, Leningrad District, U.S.S.R.

[1] V. V. Anisovich and M. M. Giannini, Report No. INFN-Genova, 1990 (unpublished); Z. Phys. C (to be published).

[2] V. V. Anisovich, in *Proceedings of the International Europhysics Conference on High Energy Physics,* Madrid, Spain, 1990, edited by F. Barreiro and C. Lopez [Nucl. Phys. B (Proc. Suppl.) **16**, 443 (1990)].

[3] A. Mueller, in *Proceedings of the 17th Rencontre de Moriond on Elementary Particle Physics. II. Elementary Hadronic Processes and New Spectroscopy,* Les Arcs, France, 1982, edited by J. Tran Thanh Van (Editions Frontières, Gif-sur-Yvette, 1982).

[4] S. J. Brodsky, in *Multiparticle Dynamics 1982,* Proceedings of the 13th International Symposium, Volendam, The Netherlands, 1982, edited by E. W. Kittel, W. Metzger, and A. Stergiou (World Scientific, Singapore, 1982).

[5] A. De Rújula, H. Georgi, and S. L. Glashow, Phys. Rev. D **12**, 147 (1975).

[6] N. Isgur and G. Karl, Phys. Rev. D **18**, 4187 (1978); **19**, 2653 (1979).

[7] W. Blask, M. G. Huber, and B. Metsch, Z. Phys. A **326**, 413 (1987); K. S. Sharma, W. H. Blask, B. Metsch, and M. G. Huber, Phys. Rev. Lett. **62**, 2913 (1989).

[8] V. V. Anisovich, M. N. Kobrinsky, J. Nyiri, and Yu. M. Shabelski, *Quark Model and High Energy Collisions* (World Scientific, Singapore, 1985).

[9] A. Capella *et al.*, Z. Phys. C **3**, 329 (1980).

[10] G. Cohen-Tannoudji, A. El Hassouni, J. Kalinowski, O. Napoly, and R. Peschanski, Phys. Rev. D **21**, 2699 (1980).

[11] P. V. Landshoff and O. Nachtmann, Z. Phys. C **35**, 405 (1987).

[12] L. G. Dakhno and N. N. Nikolaev, Nucl. Phys. **A436**, 653 (1985).

[13] N. N. Nikolaev, Z. Phys. C **32**, 537 (1986).

[14] D. Cline, F. Halzen, and J. Luthe, Phys. Rev. Lett. **31**, 491 (1973).

[15] S. D. Ellis and M. B. Kislinger, Phys. Rev. D **9**, 2027 (1974).

[16] P. L'Heureux, B. Margolis, and P. Valin, Phys. Rev. D **32**, 1681 (1985).

[17] T. K. Gaisser and F. Halzen, Phys. Rev. Lett. **54**, 1754 (1985).

[18] K. Kajantie, P. V. Landshoff, and J. Lindfors, Phys. Rev. Lett. **59**, 2527 (1987).

[19] L. Durand and H. Pi, Phys. Rev. D **40**, 1436 (1989).

[20] B. Z. Kopeliovich, N. N. Nikolaev, and I. K. Potashmikova, Phys. Rev. D **39**, 769 (1989).

[21] I. Sarcevic, S. D. Ellis, and P. Carruthers, Phys. Rev. D **40**, 1446 (1989).

[22] T. K. Gaisser and T. Stanev, Phys. Lett. B **291**, 375 (1989).

[23] L. N. Lipatov, Zh. Eksp. Teor. Fiz. **90**, 1536 (1986) [Sov. Phys. JETP **63**, 904 (1986)].

[24] M. G. Ryskin, in *Elastic and Diffractive Scatterings,* Proceedings, Evanston, Illinois, 1989, edited by M. M. Block and A. R. White [Nucl. Phys. B (Proc. Suppl.) **12**, 40 (1990)].

[25] G. 't Hooft, Nucl. Phys. **B72**, 461 (1974).

[26] G. Veneziano, Nucl. Phys. **B117**, 519 (1976).

[27] I. I. Balitsky, L. N. Lipatov, and V. S. Fadin, in Proceedings of the Fourteenth LNPI Winter School, Leningrad, 1979 (unpublished), Vol. 1, p. 109.

[28] L. G. Dakhno and V. A. Nikonov, Yad. Fiz. **51**, 280 (1990) [Sov. J. Nucl. Phys. **51**, 127 (1990)].

[29] V. V. Anisovich and L. G. Dakhno, Nucl. Phys. **B85**, 208 (1975).

[30] A. S. Carroll *et al.*, Phys. Lett. **61B**, 303 (1976).

[31] L. A. Fajardo *et al.*, Phys. Rev. D **24**, 46 (1981).

[32] The authors thank N. U. Nikolaev for clarifying some statements of Ref. [13].

[33] V. N. Gribov, Zh. Eksp. Teor. Fiz. **56**, 892 (1969) [Sov. Phys. JETP **29**, 483 (1969)].

[34] J. Pumplin and M. Ross, Phys. Rev. Lett **21**, 1778 (1968).

[35] V. V. Anisovich, L. G. Dakhno, and P. E. Volkovitsky, Phys. Lett. **42B**, 224 (1972).